Applied Catalysis B: Environmental 196 (2016) 57–67

Contents lists available at ScienceDirect

Applied Catalysis B: Environmental

journal homepage: www.elsevier.com/locate/apcatb

A green approach assembled multifunctional Ag/AgBr/TNF membrane for clean water production & disinfection of bacteria through utilizing visible light

Chengli Tang[a,d,1], Hongwei Bai[a,b,*], Lei Liu[a], Xiaoli Zan[c], Peng Gao[a], Darren Delai Sun[a,**], Wei Yan[d,**]

[a] School of Civil and Environmental Engineering, Nanyang Technological University, 50 Nanyang Avenue, Singapore 639798, Singapore
[b] Energy Research Institute @NTU (ERI@N), Nanyang Technological University, Singapore 737141, Singapore
[c] School of Materials Science and Engineering, Nanyang Technological University, 50 Nanyang Avenue, Singapore 639798, Singapore
[d] Department of Environmental Science and Engineering, Xi'an Jiaotong University, Xianning West Road 28#, Xi'an 710049, China

ARTICLE INFO

Article history:
Received 2 March 2016
Received in revised form 2 May 2016
Accepted 11 May 2016
Available online 12 May 2016

Keywords:
Ag/AgBr/TNF composites
Disinfection of bacteria
Multifunctional membrane
Visible light
Water treatment

ABSTRACT

In order to realize the ideal water treatment in a green and energy saving manner, TiO_2 based multifunctional membrane proved to be a promising approach owing to its capability in utilizing visible light for photocatalytic pollutant degradation and disinfection of bacteria. However, few studies were found about the investigation of antibacterial abilities arising from the intrinsic properties of membrane and its minor composition. Here, a multifunctional membrane was created via a green approach to integrate the merits of hierarchical Ag/AgBr/TNF composites with micro-/-nano porous structures, the intrinsic antibacterial abilities of Ag, and the visible light absorption capability of AgBr. The synergy effects made it being a promising multifunctional membrane for concurrent water filtration and disinfection in a sustainable way. Through a versatile characterization techniques of FESEM, XRD, TES, XPS, and UV-vis spectrometer, the morphology, structure and surface properties of the well prepared Ag/AgBr/TNF multifunctional membrane was thoroughly studied to reveal the deep mechanism behind the high flux, high photocatalytic degradation and disinfection efficiency under visible light. It indicates that the Ag/AgBr/TNF multifunctional membrane exhibited better photocatalytic activity, higher water permeate flux, and higher disinfection abilities over commercial P25 membrane under visible light. Besides the deep mechanism elaborated, the key factors in terms of predominant oxidative species was also exploited in details. This further solidify the broad future of the developed multifunctional membrane. In view of the roaring demand of advanced water treatment and disinfection technology, it is reasonable to believe our developed visible light responsive Ag/AgBr/TNF multifunctional membrane will show great significances to a green and clean future.

1. Introduction

Human beings have been threatened by severe and global water crisis [1,2]: (1) fast depletion of fresh and accessible water resource, (2) dirty, toxic and polluted water raging, and (3) water-borne diseases transmitting [3]. Global water resources are constant through natural cycles or transformation, while the fresh and clean water resources is a minor part and are being depleted or polluted at an unprecedented rate accompanying the fast urbanization and industrialization [4,5]. The increasing global populations further accelerated the consumption of clean water, and the climate change will cause adverse effect on this trend [6,7]. The unstrained and greedy human activities poured lots of toxic and misplaced pollutants into natural fresh water bodies like surface rivers and underground waters resulting in the heavy water pollution [8,9]. Obviously, there is a contradiction between clean water shortage and increasing wastewater, which is not only the cause but also the effect of water crisis [10]. As thus it is an ideal way to solve the conflict through technologically purifying the wastewater in terms

* Corresponding author at: School of Civil and Environmental Engineering, Nanyang Technological University, 50 Nanyang Avenue, Singapore 639798, Singapore.
** Corresponding authors.
E-mail addresses: hwbai@ntu.edu.sg, baihw0001@gmail.com (H. Bai), DDSUN@ntu.edu.sg (D.D. Sun), yanwei@mail.xjtu.edu.cn (W. Yan).
[1] Present address: College of Mechanical and Electrical Engineering, Jiaxing University, Jiaxing 314001, P.R. China.

http://dx.doi.org/10.1016/j.apcatb.2016.05.023
0926-3373/

of pollutants removal and disinfection of bacteria into clean water to guarantee the water security issue [11–15].

In the past years, lots of technologies have been developed for wastewater purifications such as the conventional physical, chemical and biological methods [2]. These traditional methods proved to play a significant role in wastewater treatment and environmental remediation [16–18]. However, these methods are always featured as high energy consumption, low efficiency, low productivity and secondary pollution, which cannot meet the stringent wastewater discharge requirements, high living standards, cost-effective, green and sustainable approaches after considering the even severer global energy crisis [19–21].

Since 1960s, polymer based membrane filtration has become a dominant water treatment technology by rejecting pollutants to produce high quality water at a very competitive cost [22]. However, the intrinsic hydrophobic polymer membrane is easy to be fouled owing to the accumulation of pollutants and bacteria on the surface or in the pores of membrane becomes a bottleneck limiting the broad application of membrane, as it may cause lots of adverse effects such as poorer water quality, lower water productivity, energy-intensive, shorter membrane lifespan and potential secondary pollution [23–25]. To address the membrane fouling issue, our group has developed a novel and sustainable approach in the past years [8,23,26–28]. Basically, two strategies were developed and well proved: (1) change the surface property of hydrophobic membrane into hydrophilic membrane by using inorganic TiO_2 nanofiber materials for high permeate flux [29–31], and (2) multifunctionalize the membrane through incorporating the functions of TiO_2 adsorption/photodegradation of organics matters, and bacteria disinfection for process fouling control and mitigation [32–34]. Following these, we have developed versatile TiO_2 multifunctional membranes and applied them for practical water treatment and disinfections. In particular, well-tailored TiO_2 nanostructure is one of the most successful platform for multifunctional membrane as its unique features in terms of increasing more hierarchical micro-/-nano porous, reducing the intrinsic resistance of membrane and building up more reaction sites for photocatalytic reaction occurring and pollutants adsorption [35–37].

Hierarchically structured TiO_2 membrane is famous for photocatalytic degradation of organic matters, killing bacteria and filtration. However the limiting factor for TiO_2 photocatalytic broad application lies in the limited UV which accounts for less than 4% of full solar spectrum [37], but the only energy source to excite TiO_2 to generate electrons and holes for photocatalysis [33].

Starting from a point of practical engineering application, energy-efficient photocatalysts are highly demanded to effectively utilize the visible light that constitutes 43% of the total sunlight [37]. Hence, it is important to develop a visible light responsive photocatalyst [38–40], and some efforts have been devoted to developing "second-generation" TiO_2 [41] and other narrow band gap semiconductors [42,43] that can absorb visible light. In recent years, numerous interest has been paid to designing Ag/AgX (X = Cl, Br, I) composite materials for specific applications such as bacteria destruction and degradation of organic pollutants in water [44–51].

Although some studies reported the integration of Ag, AgBr with TiO_2 in the form of nanoparticles, spheres, or one dimensional (1D) materials, there is few ideal approach to maximize the best performance of Ag, AgBr and TiO_2 through complete mixing at molecular level. Low temperature hydrothermal reaction provides a good platform to solve this problem by guaranteeing the sufficient and well mixing of Ag, AgBr and TiO_2 precursor from the level of molecular chemistry, this will guarantee the close contact between Ag, AgBr and TiO_2 to promote the fast electrons transfer at a minimal electricity resistance [12,52–54].

Here, we report a tertiary Ag/AgBr/TiO_2 nanofiber (Ag/AgBr/TNF) membrane platform to fully exploit the merits of (1) hierarchical scaffold nanofiber porous structures for high permeate flux, (2) multifunctional pollutants removal and disinfection by adsorption, rejection and degradation by Ag/AgBr/TNF under visible light, and (3) maximizing the advantages of membrane and photocatalysis while completely solving the issues of membrane fouling and catalyst recovery. Because of the close contact and well mixing of AgBr with TiO_2, the visible light absorbing capability and high photocatalytic efficiency of AgBr/TiO_2 will be further accelerated by Ag [50]. While, the intrinsic antibacterial ability of Ag will also enhance the disinfection of bacteria simultaneously. All these unique merits will lead to a sharp weapon to solve the wastewater treatment, clean water production and disinfection of bacteria issues in practical engineering applications.

2. Materials and methods

2.1. Materials

Cetyltrimethylammonium bromide (CTAB), silver nitrate ($AgNO_3$), dimethylsulfoxide (DMSO), ethylenediaminetetraacetic acid (EDTA), and salicylic acid (SA) were purchased from Sigma Aldrich. Commercial TiO_2 powder (Degussa P25) (P25 NP) was obtained from Germany Degussa Corporation (BET surface area, *ca.* 50 m^2/g; particle size, 25 nm). All the above reagents were of AR grade and used as received. Deionized (DI) water was used throughout this study. *Escherichia coli* (*E. coli*) K12 ER2925 was purchased from New England Biolab.

2.2. Fabrication of TiO_2 nanofibers (TNF) and synthesis of Ag/AgBr/TNF composites

A facile low temperature hydrothermal method was used to synthesize TNF with dissolving P25 NPs into 10 mol/L NaOH [55]. The resultant solution was transferred into a Teflon-lined autoclave and stored in the electronic oven for 48 h at 180 °C. After naturally cooling down, white precipitation formed at the bottom was recovered and repeatedly washed by 0.1 mol/L HCl solution and then DI water with the assistance of ultrasound. The TNF was gained after calcination of the neutralized product at a temperature of 600 °C.

The product of Ag/AgBr/TNF was synthesized by a modified deposition-precipitation method as mentioned in literature [56]. Typically, 0.1 g of TNF was ultrasonicated in 50 mL of DI water to disperse it evenly. Then, 0.12 g of CTAB was added to this suspension, and the mixture was stirred magnetically for 2 h to get a homogeneous solution. After that, 2 mL of 0.6 mol/L diamminesilver(I) hydroxide($Ag(NH_3)_2OH$) was quickly added to the mixture. This solution was aged with stirring for 20 h and then filtered, washed with water, and dried at 60 °C. The final Ag/AgBr/TNF photocatalysts were obtained by calcination at 500 °C in air for 3 h.

2.3. Fabrication of multifunctional Ag/AgBr/TNF membrane

With referring to our previous studies [27], identical amount of as-synthesized Ag/AgBr/TNF composite materials were suspended in DI water and then filled into a filtration cup at the bottom of which a commercial cellulose acetate (CA) membrane from Millipore was mounted [8,37]. The substrate CA membrane is 47 mm in diameter and has a pore size of 0.45 μm. By using a dead-end filtration setup as described in Fig. S1 (Supporting information (SI)), the synthesized Ag/AgBr/TNF composite were uniformly assembled onto the surface of CA and formed a hierarchically structured new functional layer. Under the given operating pressure, the Ag/AgBr/TNF is well assembled onto the CA membrane and is stable for concurrent water purifications.

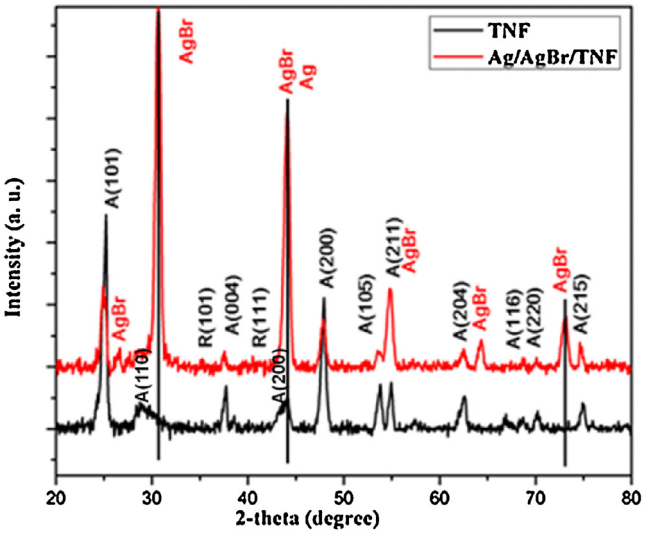

Fig. 1. XRD patterns of the bare TNF(a) and Ag/AgBr/TNF(b) in which A is the anatase phase and R is the rutile phase of TiO_2.

2.4. Characterization

Powder X-ray diffraction (XRD) was performed with Cu Kα radiation on a Bruker D8 Advance X-ray diffract meter operating at 40 kV and 30 mA with scanning rate of 2°/min from 5 to 80°. The morphologies of the synthesized materials were investigated using a field-emission scanning election microscope (FESEM) Jeol JSM-6340F (Japan) operated at 5 kV. Energy dispersive X-ray (EDS) measurement was conducted using the EDAX system attached to the same field emission scanning electron microscopy with carbon tape and platinum sputtering used for the sample preparations. Transmission electron microscopy (TEM) was performed on a Jeol JEM-2100F (Japan) operated at 200 kV. The samples for the analysis were prepared by dropping TNF and Ag/AgBr/TNF suspensions. The chemical states of the products were studied using the X-ray photoelectron spectroscopy (XPS) measurement performed on Axis Ultra, Kratos (UK) at monochromatic AlKα radiation (150 W, 15 kV and 1486.6 eV). And charge-referenced using C 1s core level at 284.8 eV for the adventitious carbon. The UV–vis absorption spectra were recorded use an Evolution 300 Spectrophotometer (UV-1700 Shimadzu). The porosities of the TNF and Ag/AgBr/TNF composites were determined by the N_2 adsorption/desorption isotherm method by using a Micromeritics ASAP 2040 system at liquid nitrogen temperature (77 K). Before the measurement, each 0.1 g sample was degassed under vacuum for 6 h at 250 °C. Pore volume and size distributions were derived from the desorption branches of the isotherms by the Barrett-Joyner-Halenda (BJH) model, and the Brunauer-Emmett-Teller (BET) equation was used to calculate the specific surface areas from the adsorption data.

2.5. The investigation of photocatalytic activity

The photocatalytic activity of the Ag/AgBr/TNF membrane was evaluated with Methylene Blue (MB) as probe pollutant in a dead-end membrane filtration system setup (Fig. S1, Supporting information (SI)) as described in our previous work [10,27]. For the photodegradation, 50 mL of MB solution (10 ppm) was filled into the filtration cup, the MB solution in the filtration cup was kept in dark for 0.5 h to reach the adsorption equilibrium before switching on the visible light simulator (Xenonarc lamp, Newport Oriel, 80 mW/cm^2). The trans-membrane pressure (TMP) was maintained around 0.05 MPa during the whole processes. 3 mL permeates were collected to measure the UV-absorption value at 605 nm at an interval of 10 min for 60 min. As a contrast, the photocatalytic degradation of MB by P25 NP and TNF deposited membrane were also conducted under the same conditions. The degradation of MB under visible light irradiation without membrane was also tested.

To explore the photocatalytic mechanism, especially the role of electrons and holes, experiments on the Ag/AgBr/TNF membrane were carried out in the presence of DMSO (20 mM)and EDTA

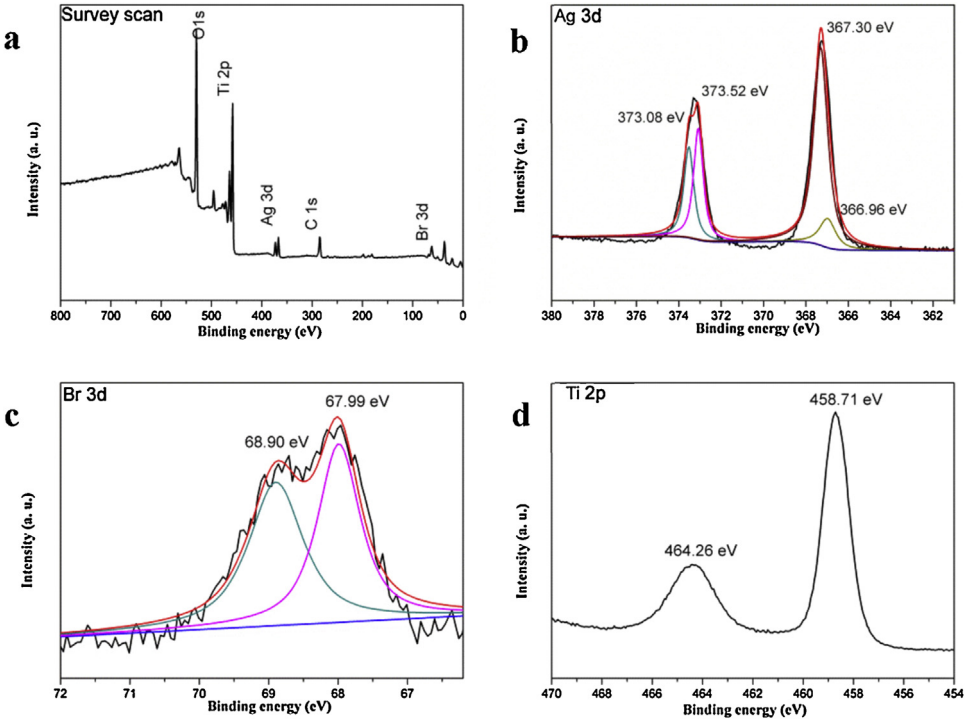

Fig. 2. Survey scan XPS spectra (a) and high-resolution XPS spectra of Ag 3d (b), Br 3d (c) and Ti 2p (d) regions for the Ag/AgBr/TNF nanocomposites.

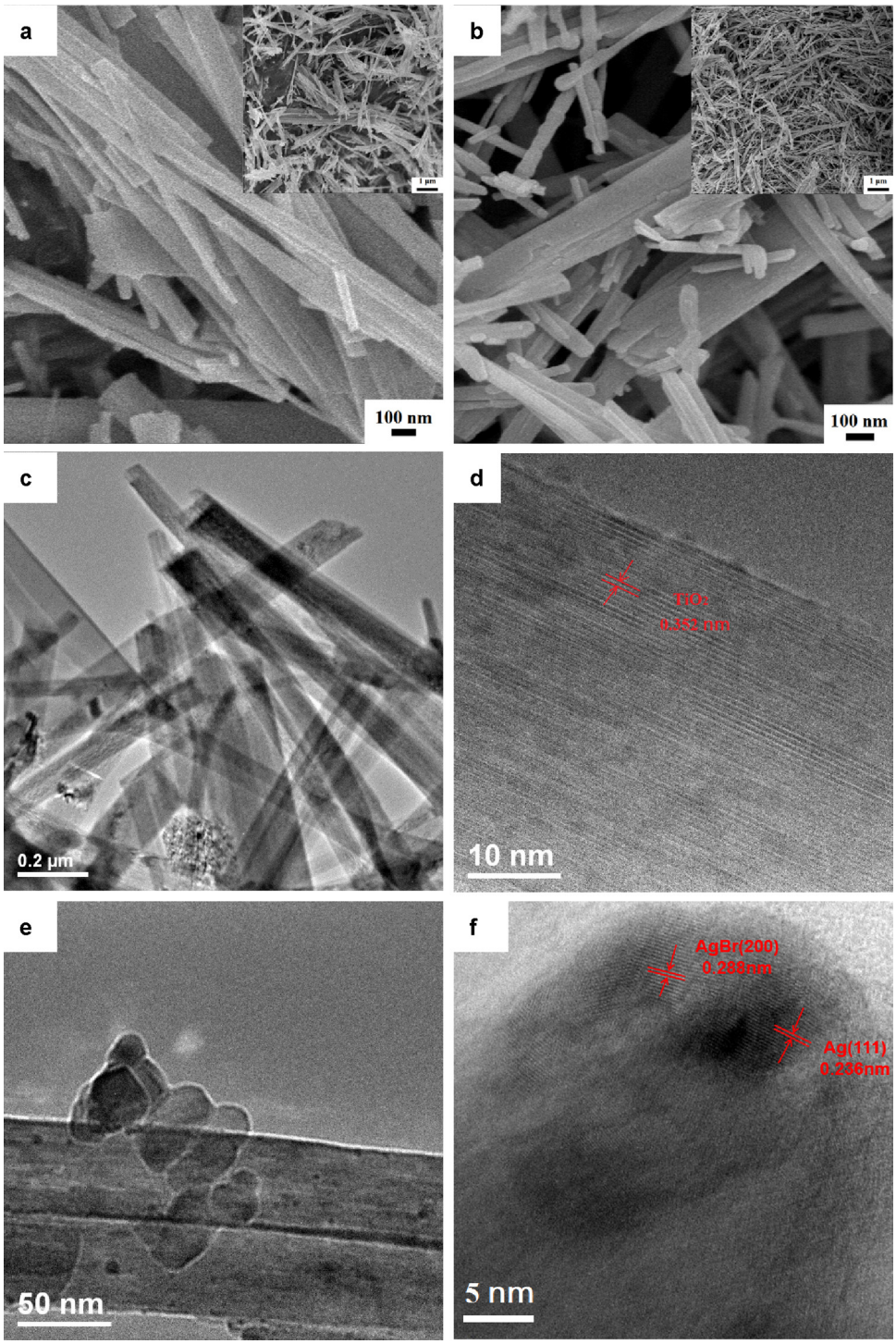

Fig. 3. FESEM images of the as-prepared TNF (a) (insert low magnification) and Ag/AgBr/TNF (b) (insert low magnification), TEM images of the as-prepared TNF (c) and Ag/AgBr/TNF (e), HRTEM images of the as-prepared TNF (d) and Ag/AgBr/TNF (f).

(20 mM). Control experiment of DMSO (20 mM) and EDTA (20 mM) without membrane was carried out at the same time.

2.6. Photocatalytic disinfection of bacteria

E. coli was chosen as the model pathogen for antibacterial activity tests. *E. coli* was cultivated in Luria-Bertani (LB) nutrient solution at 37 °C for 18 h to get the exponential growth phase. The cells were harvested by centrifugation and washed with saline solution (0.9% NaCl) to remove residual macromolecules. All glass apparatuses and solutions used in the experiments were autoclaved at 121 °C for 20 min to ensure sterility.

In consideration of the interceptive role of the membrane to *E. coli*, the photocatalytic disinfection performance was investigated in a static system without circulation but only a magnetic stirring (the dotted bordered rectangle in Fig. S1). The disinfection activity of the Ag/AgBr/TNF composites was evaluated by assessing the inactivation of *E. coli* under visible light irradiation. A visible light simulator (Xenonarc lamp, Newport Oriel, 80 mW/cm^2) was used as the light source. 50 mL water containing *E.coli* (10^7 CFU/mL) was

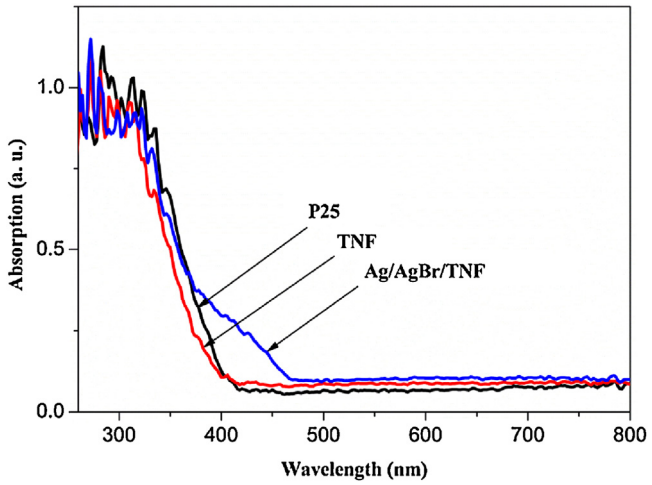

Fig. 4. UV–vis spectra of P25, TNF and Ag/AgBr/TNF.

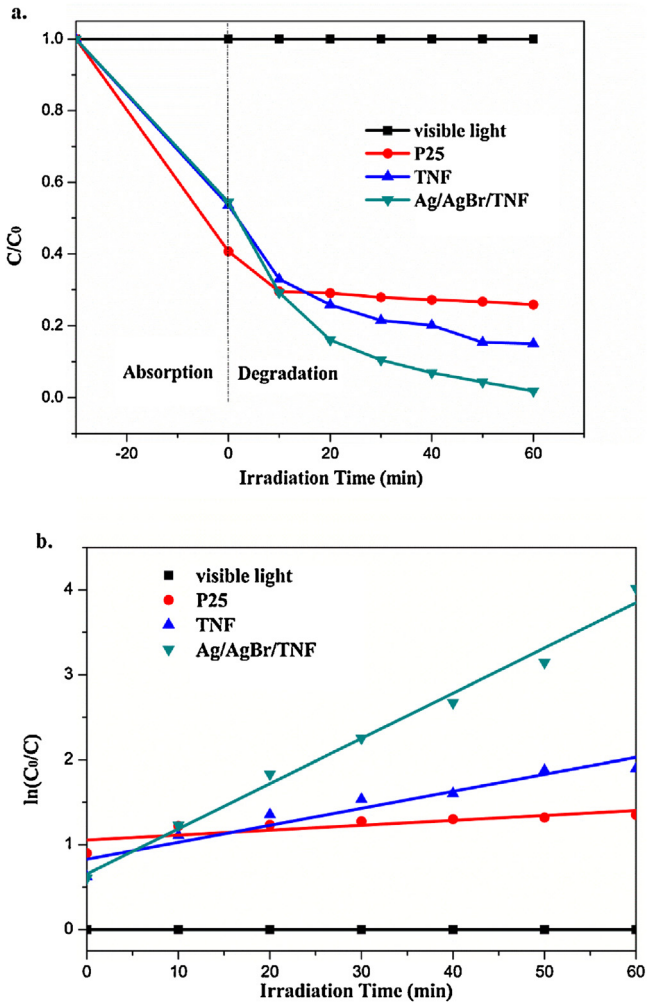

Fig. 5. Temporal course of the decrease in the MB concentration (a) and ln(c_0/c) (b) with visible light irradiation time use different membranes. (Experimental conditions: MB concentration 10 ppm).

mixed with the Ag/AgBr/TNF materials. At irradiation time of 10, 20, 30, 40, 50, 60 min, an aliquot of the solution was immediately diluted with PBS and an appropriate dilution of the sample was spread on nutrient agar and incubated at 37 °C for 24 h. The number of colonies formed was counted to determine the number of viable cells. All the above experiments were conducted in triplicates to get the average result. Control experiments with P25 NP and TNF was also done at the same time. To investigate the effect of visible light irradiation, control experiments in dark were tested. The mechanism investigation experiments were also carried out to explore the role of electrons and holes in the degradation process, which followed the same procedures as in Section 2.5.

The antibacterial activity of the Ag/AgBr/TNF membrane was also tested on *E. coli* using the disk-diffusion method [37]. The disk diffusion assay was performed by placing a 10 mm Ag/AgBr/TNF membrane onto an agar plate seeded with approximately 10^7 CFU/mL of *E. coli*. After incubation at 37 °C for one day, the diameters of the inhibition zones were observed. Control experiments (P25 NP and TNF membrane) were made to check for the growth of the bacterial.

2.7. Flux performance investigation of Ag/AgBr/TNF multifunctional membrane

The flux performance of Ag/AgBr/TNF, P25 NP and pure TNF deposited membrane were investigated in the same dead-end membrane system setup (Fig. S1). This bench-scale system comprises of a membrane cell with a filtration cup volume of 60 mL. The effective membrane area was 13.4 cm^2. Pressure was provided by a compressed N_2 gas cylinder, which was connected to the filtration cup. The TMP used in experiments was 0.6 MPa. Permeate was collected and its mass was measured continuously over time using a weighing balance connected to a data logger. Data was collected every second and then averaged per minute. Permeate flux was calculated on the basis of permeate mass divided by effective surface area and filtration time, the unit is L/m^2 h (LMH).

3. Results and discussion

3.1. Materials characterizations

The phase structure of the as-prepared TNF and Ag/AgBr/TNF has been analyzed by the XRD technique. From the XRD patterns in Fig. 1, it knows that the pure TNF was predominantly of anatase phase, while a mixture of anatase, rutile, Ag and AgBr was formed in Ag/AgBr/TNF. Except for the diffraction peaks characteristic of anatase, the peaks at 2θ *ca.* 26.7°, 31.0°, 44.4°, 55.0°, 64.5° and 73.4° indexed to AgBr (JCPDS no. 6–438) can also be observed in Ag/AgBr/TNF [45]. The diffraction peak at *ca.*55.0° can be assigned to the (211) plane of anatase as well [53]. In addition, the diffraction peaks at about 44.4° and 64.5° can be assigned to both Ag^0 and AgBr. It is noticeable that the characteristic peak of Ag^0 at 38.1° was not found, possibly due to its low content, ultrafine particle size and high dispersion [45].

The synthesized Ag/AgBr/TNF composites were further analyzed by XPS (Fig. 2) to investigate the surface chemical structures and elemental compositions. Strong peaks of Ag 3d, Br 3d, Ti 2p and O 1s are observed in the XPS spectra of Ag/AgBr/TNF. Two typical peaks of Ag 3d located at 367.26 eV and 373.31 eV can be attributed to the Ag $3d_{5/2}$ and Ag $3d_{3/2}$ binding energies, respectively. The Ag $3d_{5/2}$ peak and $3d_{3/2}$ peak can be further divided into two different peaks. Specifically, the peaks at 367.30 eV and 373.52 eV are attributed to metallic Ag^0, and those at 366.97 eV and 373.08 eV are attributed to be Ag^+ of AgBr [45,46]. The Br 3d spectra (Fig. 2c), consists of two individual peaks Br $3d_{5/2}$ and Br $3d_{3/2}$, with binding energies 67.99 eV and 68.90 eV, respectively [45]. This reveals the successful formation of AgBr in the Ag/Agbr/TNF composites [45]. The spectra of Ti 2p in Fig. 2d shows that the binding energies of Ti $2p_{3/2}$ and Ti $2p_{1/2}$ are 458.71 eV and 464.26 eV, respectively [13]. This is ascribed to be the Ti^{4+} in the Ag/AgBr/TNF compos-

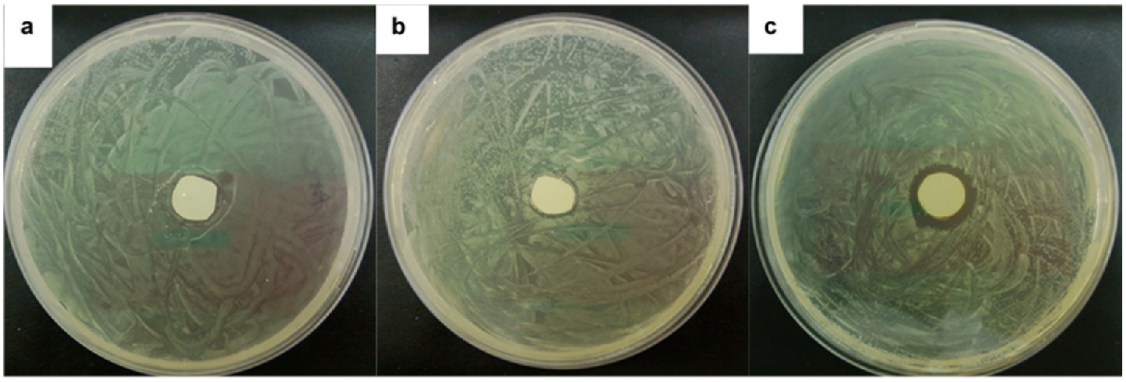

Fig. 6. Photographs of inhibition zone test results. Comparison of the P25 deposited membrane (a), pure TNF deposited membrane (b) and Ag/AgBr/TNF membrane (c).

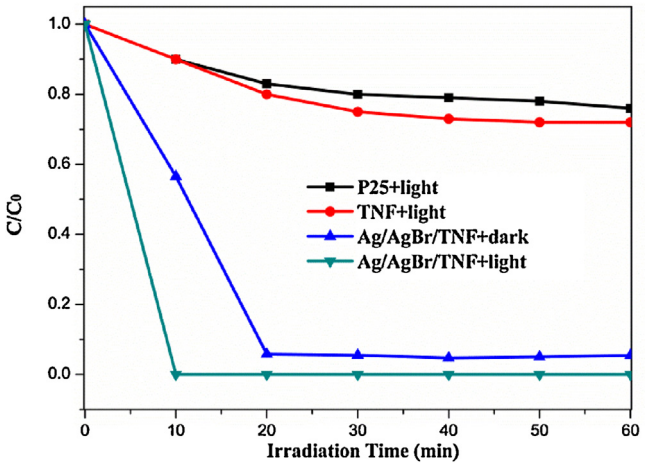

Fig. 7. Photocatalytic disinfection of *E. coli* in various conditions (initial bacterial concentration: 10^7 CFU/mL, solar intensity: 80 mw/cm^2).

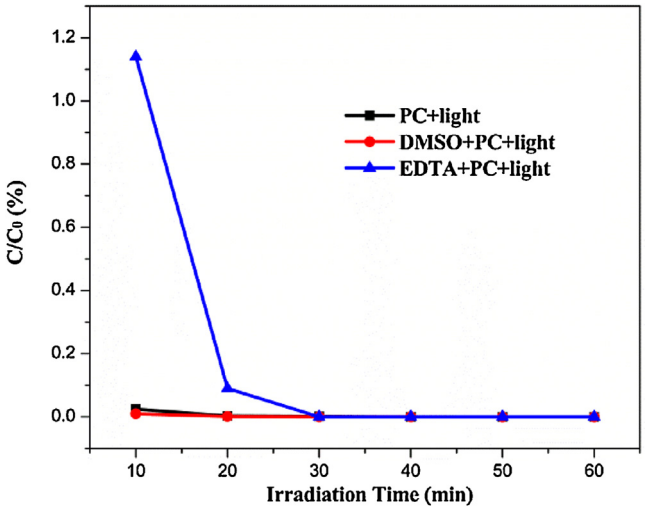

Fig. 8. Photocatalytic disinfection of *E. coli* in Ag/AgBr/TNF/visible light system in the presence of DMSO (20 mM) and EDTA (20 mM) (initial bacteria concentration: 10^7 CFU/mL, solar intensity: 80 mw/cm^2).

ites. Based on the XPS analysis, the surface contents of Ag^0, Ag^+ and Br^-ions on the surface of Ag/AgBr/TNF are calculated to be 0.80, 0.34 and 0.54 mol%, respectively. This result indicates the coexistence of metallic Ag and AgBr in the composites. It also suggests that the surface of TNF support is not completely covered by Ag^0 and AgBr species, which is favorable for the charge transfer. [46,57].

The FESEM images of TNF (Fig. 3a) and Ag/AgBr/TNF (Fig. 3b) show that there was no obvious change in the morphology after the hydrothermal treatment. The diameter of the fiber is measured to be *ca.* 65–105 nm (Fig. 3a) and the length is about a dozen μm (insert in Fig. 3a). The Ag/AgBr/TNF maintained the same fiber shape as the TNF. From the FESEM images of Ag/AgBr/TNF, a typical hierarchical structure was observed, in which: the distances between different TNFs, different AgNPs and AgBr spheres were in the range of nanomater micrometer scales. The typical hierarchical structure would create lots of benefits for higher light absorption capability, larger specific surface area and faster electron transfers for longer lifespan of photogenerated electrons and holes [10,52]. All these features would be in favor of the improvement of photocatalytic activity. More specific microscopic morphology and structure information of the as-prepared TNF and the Ag/AgBr/TNF were investigated by TEM analysis, as shown in Fig. 3c and e. The HRTEM image of TNF in Fig. 3d shows the distinct lattice fringe of $d = 0.352$ nm, which matched with the crystal graphic plane of anatase TiO_2 (101). By measuring the lattice fringes as displayed in the HRTEM image of Ag/AgBr/TNF (Fig. 3f), the resolved inter planar distances are found to be *ca.* 0.288 nm and 0.236 nm corresponding to the planes of AgBr (200) (JCPDS no. 6-438) and Ag (111) (JCPDS no. 65-2871) respectively [57]. It demonstrates the successful formation of Ag/AgBr nanojunctions in the as-synthesized Ag/AgBr/TNF composites. Additionally, Fig. 3e indicates that the surface of TNF is not completely covered by Ag and AgBr species. This is in accordance with the aforementioned XPS results. The porosities of the synthesized Ag/AgBr/TNF composites and pure TNF were further investigated by N_2 adsorption/desorption. The N_2 adsorption/desorption isotherm curve and pore size distribution curve of the synthesized Ag/AgBr/TNF and pure TNF were presented in Fig. S3a and b (Supporting information (SI)), respectively. From Fig. S3a, it is clear to see that both Ag/AgBr/TNF and TNF have typical mesoporous properties [9,12]. While the pore size distribution curve in Fig. S3b further reveals that there are at least two dominant peaks both for the Ag/AgBr/TNF and TNF materials. This further reinforces the hierarchical structure properties of Ag/AgBr/TNF and TNF as revealed by previous FESEM images in Fig. 3.

The UV–vis absorption spectra of the P25, TNF and Ag/AgBr/TNF are presented in Fig. 4. The TNF shows a slight increase in visible light absorption. After loading Ag/AgBr composite on the TNF surface, the band edge increased to about 500 nm, implying that the Ag/AgBr/TNF could absorb light in visible region. This is as a result of the visible light response property from Ag and AgBr and the unique hierarchical structure for light scattering, reflection and absorption [21,45].

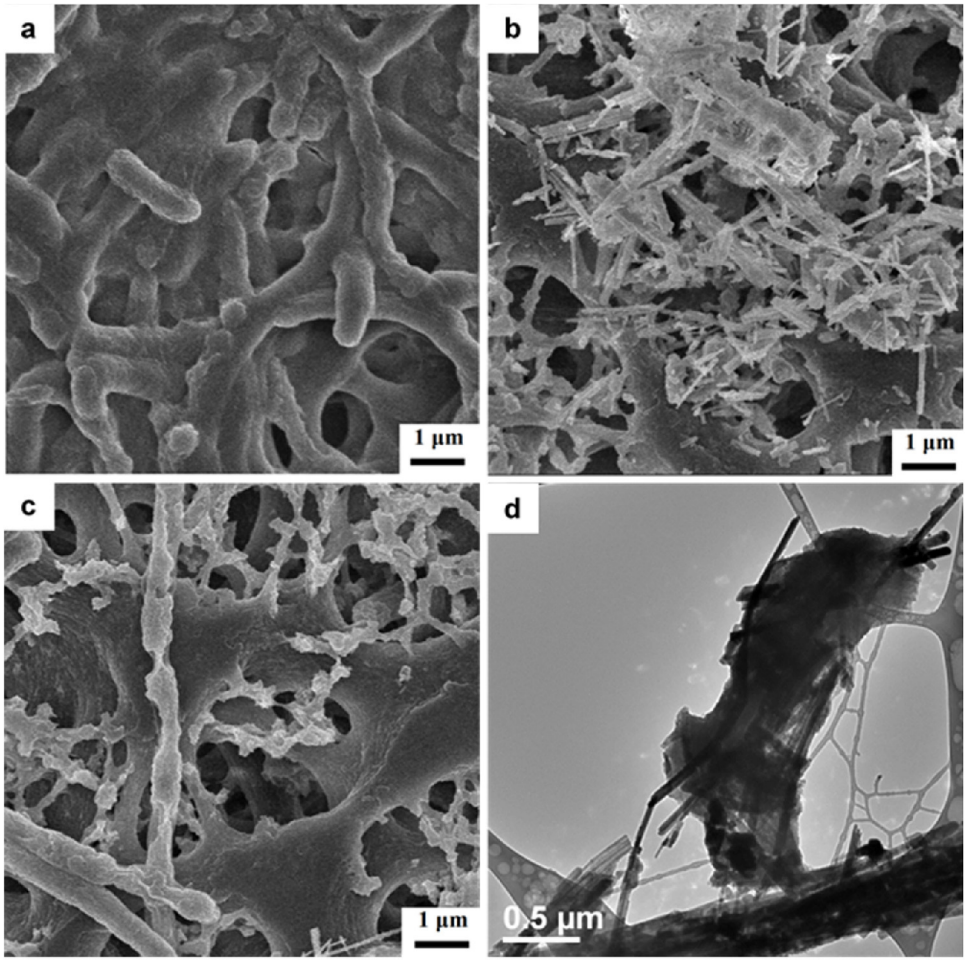

Fig. 9. FESEM images of *E. coli* (a) untreated, (b) after photocatalytic inactivation treatment with Ag/AgBr/TNF for 30 min, (c) after PC inactivation treatment with Ag/AgBr/TNF for 60 min and (d) TEM image of *E. coli* after photocatalytic inactivation treatment with Ag/AgBr/TNF for 30 min.

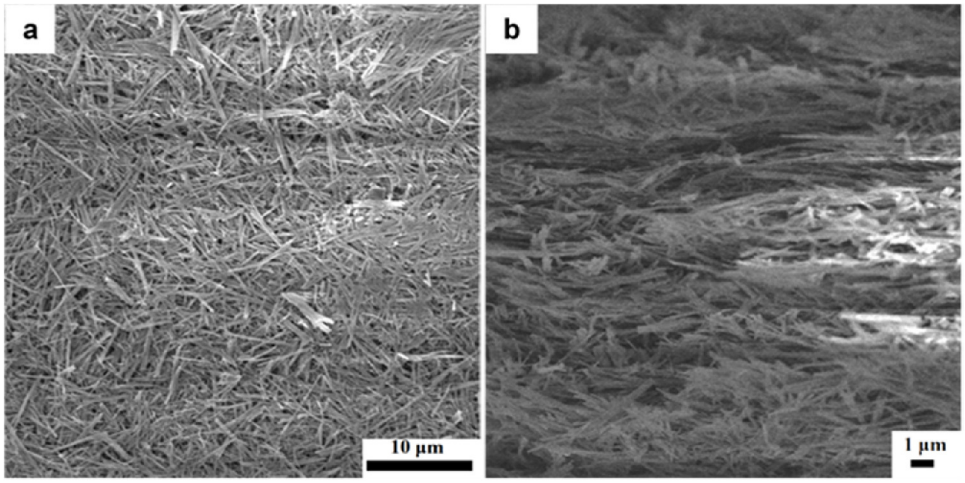

Fig. 10. FESEM images of the Ag/AgBr/TNF membrane (a) top-view and (b) cross-sectional.

3.2. Performance investigation of multifunctional Ag/AgBr/TNF membrane and mechanism revelation

3.2.1. Photocatalytic degradation of MB under visible light

The photocatalytic activity of Ag/AgBr/TNF membrane was investigated using MB as indicated organic pollutant under visible light irradiation. Fig. 5a shows the PCD results of MB at different conditions. As shown in Fig. 5a, no obvious removal of MB occurred by the visible light irradiation even after 60 min, indicating that there was no self-photosensitization process of dyes under visible light irradiation, this is similar with previous report [45]. At the same time, from Fig. 5a, we also noticed that P25 NP showed the best adsorption activity of 59.3%. The Ag/AgBr/TNF membrane showed the same adsorption capacity as the pure TNF membrane

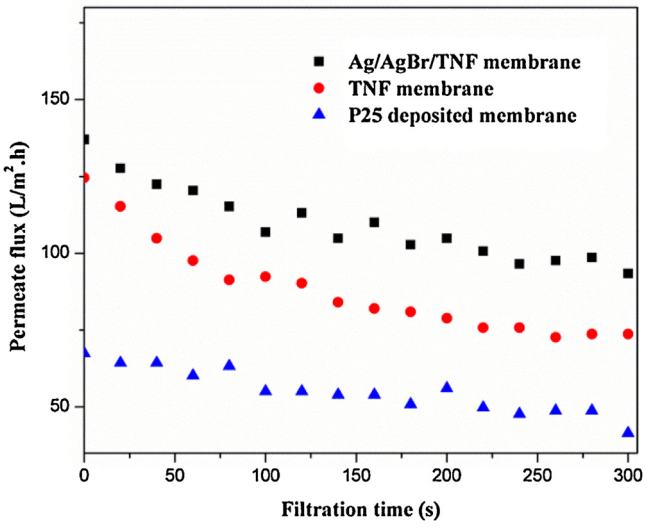

Fig. 11. Membrane flux over filtration of P25, TNF and Ag/AgBr/TNF suspensions (TMP = 0.6 MPa).

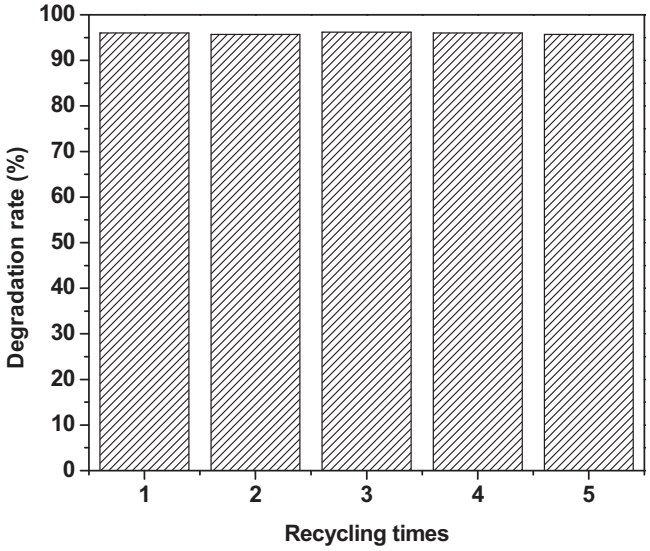

Fig. 12. Photocatalytic degradation rate of MB with the Ag/AgBr/TNF membrane in different recycling runs.

without the irradiation of visible light, even the BET specific surface area of Ag/AgBr/TNF was measured to be 67.32 m^2/g, larger than that of pure TNF of 43.2 m^2/g. This was postulated to be dominated by the weak interactions between MB and catalysts with different features [9]. As we know the adsorption of pollutants on catalyst is a critical step for their followed degradation reactions since the photocatalyst oxidation occurred mainly on the catalyst surface [58]. In the following photacatalytic degradation process, the degradation rate for P25 NP was only 36.36% at reaction time of 60 min, while the Ag/AgBr/TNF exhibited the best degradation activity of about 100%. The different removal/degradation efficiencies of Ag/AgBr/TNF and TNF before and after visible light irradiation in a comparison with P25 NP, the visible light irradiation becomes into a key factor in exciting the Ag/AgBr/TNF and promoting the fast photocatalytic degradation of MB [45], even the BET areas of Ag/AgBr/TNF and TNF were quite similar. This is due to the strong absorption in visible region caused by Ag/AgBr nanocomposites deposited on the TNF surface. Meanwhile, the large specific surface area of the tertiary Ag/AgBr/TNF composites also offers the most reaction sites for pollutant attachments and reactions smoothly in a comparison to pure P25 NP and TNF [27].

The photocatalytic degradation of MB as a function of the irradiation time in the presence of P25 NP, TNF and Ag/AgBr/TNF can be described by the first-order kinetic reaction as follows [55]:

$$\mathbf{r} = -\frac{\mathbf{d_{C_t}}}{\mathbf{d_t}} = \mathbf{k_{app} C_t} \quad \text{(E1)}$$

Accordingly,

$$-\mathbf{ln}\left(\frac{\mathbf{C_t}}{\mathbf{C_0}}\right) = \mathbf{k_{app} t} \quad \text{(E2)}$$

where r is the degradation rate of MB, C_t is the concentration of MB, k_{app} is the apparent reaction rate constant, t is the reaction time.

The data in Fig. 5a could be satisfactorily analyzed by the first-order kinetic Eq. (E2) to obtain the rate constant, the results are shown in Fig. 5b. The k_{app} for P25, TNF and Ag/AgBr/TNF are 0.0058, 0.02003 and 0.05323, respectively. This result indicates that a relatively fast degradation rate was achieved when using the TNF membrane instead of P25, because the porous structure of TNF membrane is easy for light reflection and scattering as thus resulting in slightly better light absorption capability over pure P25 NP. Furthermore, the Ag/AgBr/TNF showed a significantly enhanced photocatalytic activity compared to the pure TNF membrane, this is attributed to be the greater visible light absorption capability endowed by AgBr. Meanwhile, the tertiary structure among Ag, AgBr and TiO_2 has the bandgap difference and will also favor the fast electron transfer and charge separation for longer lifespan of generated electrons and holes [13,27].

3.2.2. *Disinfection of* E. coli

3.2.2.1. Inhibition zone test. In order to investigate the intrinsic chemical antibacterial strength of the AgNPs and test the anti-biofouling capability of multifunctional Ag/AgBr/TNF membrane, a standard Kirbye Bauer approach was applied. *E. coli* was inoculated with Ag/AgBr/TNF membrane on agar plates for 24 h. P25 NP and TNF deposited membranes were also investigated as a comparison. The results in Fig. 6 clearly show that there was no bacteria growth around the Ag/AgBr/TNF membrane, indicating that some amount of Ag^+ ions released from the membrane restrained the bacteria growth [59]. However, there was no inhibition zone around P25 NP membrane and TNF membrane. These results indicated that Ag^+ ions played an important role in the disinfection property of Ag/AgBr/TNF membrane, which was in good agreement with similar published work of Ag decorated ceramic composite [59]. These results also implied the excellent anti-biofouling property of Ag/AgBr/TNF multifunctional membrane.

3.2.2.2. Photocatalytic disinfection of E. coli. Photocatalytic disinfection of bacteria were carried out in a static system without circulation but only a magnetic stirring (the dotted bordered rectangle in Fig. S1), the results are shown in Fig. 7. Both of the P25 NP and TNF did not show obvious antibacterial capability in the absence of visible light irradiation, implying that TiO_2 itself is not toxic to the bacteria. Different from the result in earlier work [41] where neither pure TNF nor Ag/AgBr/TNF in the dark showed any bacterial effect on *E. coli*, the bacterial survival rate on Ag/AgBr/TNF decreased dramatically to 95% after 60 min in the dark. These results reveal that the Ag/AgBr nanocomposites on the Ag/AgBr/TNF composites had excellent antibacterial capacity.

In the presence of visible light irradiation, the P25 NP and TNF exhibited antibacterial activity on *E. coli*. The Ag/AgBr/TNF showed 100% of inactivation after 40 min of visible light irradiation. Compared with the 95% of inactivation rate after 60 min in the dark, visible light irradiation obviously enhanced the bacterial activity of multifunctional Ag/AgBr/TNF membrane. Two reasons are pos-

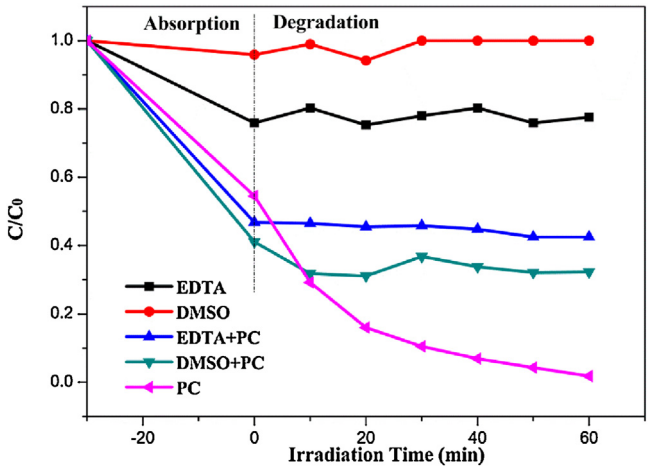

Fig. 13. Photocatalytic degradation of MB in Ag/AgBr/TNF membrane/visible light system in the presence of DMSO (20 mM) and EDTA (20 mM) (Control experiment was carried out at 20 mM DMSO and 20 mM EDTA without membrane, visible light intensity: 80 mw/cm^2).

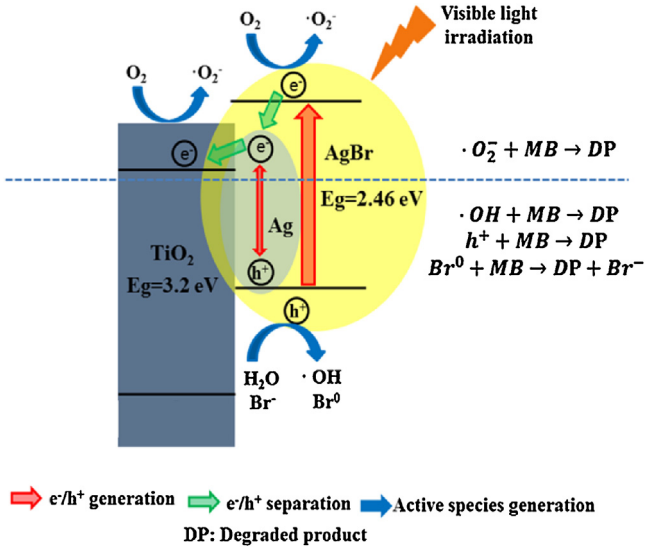

Fig. 14. Schematic diagram of the proposed photocatalytic mechanism over the Ag/AgBr/TNF membrane under visible light irradiation.

tulated: (1) although the TiO_2 is not toxic in the dark, it showed antibacterial activity under visible light irradiation; and (2) the other more important reason for the enhanced antibacterial activity is that there are photogenerated electron/hole pairs in the visible light, which can generate reactive oxygen species to inactivate the bacteria [9,59]. The scavenger test results in Fig. 8 shows that the addition of DMSO to the system has certain inhibition effect on the antibacterial activity of the Ag/AgBr/TNF. This result indicates that the photogenerated holes in the Ag/AgBr/TNF under visible light irradiation played a more important role in the antibacterial process than that of electrons. The detailed reason will be explained in the later section of mechanism revelation. Here, it is still worthy to note the significance of the intrinsic antibacterial property of Ag/AgBr composites in the dark, and it will promote the photocatalytic disinfection capability enhancement of multifunctional Ag/AgBr/TNF membrane after being excited by visible light [13,45].

3.2.2.3. E. coli *morphology analysis.* The changes in the morphology of *E. coli* at different moment of irradiation were observed as shown in Fig. 9. Fig. 9a clearly shows the appearance of *E. coli* before reaction, in which the characteristics of *E. coli* are the well-defined cell wall. In the bactericidal process the *E. coli* tends to be adsorbed on the Ag/AgBr/TNF surface (Fig. 9b). The good adsorption capacity for *E. coli* is beneficial to the bactericidal activity because of the close contact of Ag/AgBr/TNF and *E. coli*. TEM image in Fig. 9d also shows that the cell is surrounded by Ag/AgBr/TNF. The sharp tips of TNF in the Ag/AgBr/TNF composites materials also would facilitate the disinfection process through penetrating into the cell wall of *E.coli* as found in our previous report [9]. After 60 min of visible light irradiation, the morphology of the *E. coli* greatly changed (Fig. 9c). The outer membrane was guessed to be firstly decomposed and then the cell wall and cell membrane from exterior to interior would also be gradually damaged by various reactive species (like •OH radical, HO_2• radical and so on) as a result of photogenerated electrons and holes [47,56], the bacteria showed obvious shrinkage and distortion, indicating the inactivation of the *E. coli*, similar to many previous findings [27,37,60]. The decomposed bacteria indicates that the outer membrane even the cell wall and cell membrane was gradually damaged, which would lead to the leakage of the interior component [47,56], and subsequently the death of the bacteria. The contact of Ag/AgBr/TNF and *E. coli* facilitated the inactivation of *E. coli*, which is the reason why the membrane showed antibacterial property in the dark [9,59].

3.3. Flux performance and practical use applicability

Fig. 10a and b shows FESEM images of surface and cross section of the multifunctional Ag/AgBr/TNF membrane. The cross section FESEM shows 3D interconnected porous scaffold structure of the membrane, which is beneficial for water to pass through [27]. The flux performance of the Ag/AgBr/TNF membrane was determined using the lab-scale dead-end apparatus as shown in Fig. S1. Fig. 11 displays the relationships between permeate flux and filtration time (TMP = 0.6 MPa) in the P25 NP, pure TNF and multifunctional Ag/AgBr/TNF membrane. With the same TMP, the P25 deposited membrane showed significant lower flux compared to TNF membrane and Ag/AgBr/TNF membrane. The permeate flux of Ag/AgBr/TNF membrane was nearly 2 times higher than that of P25 NP deposited membrane. These results illustrated that 1D TNF structured porous membrane were favorable to maintain higher and constant permeate flux over P25 NP, as the dense layer formed by P25 NP caused the great flux reduction [23]. This was due to the rapid deposition of P25 NP onto the membrane surface to form a fouling layer instead of the formation of a multifunctional layer [23]. It is interesting to notice that the multifunctional Ag/AgBr/TNF membrane showed even higher flux than that of TNF membrane. This is ascribed to the decoration of Ag/AgBr on the TNF surface, which can increase the roughness and porosity of TNF surface [8]. The resultant Ag/AgBr/TNF composites build up a hierarchical scaffold membrane structure, as thus a highly porous and loose membrane functional layer easy for water passing through and lowering membrane intrinsic resistant but still retaining the pollutants adsorption and rejection capability (the schematic diagram illustrated in Fig. S2) [27].

3.4. Stability and practical reusability of multifunctional Ag/AgBr/TNF membrane

Besides the excellent photocatalytic activity, the stability and reusability of the multifunctional membrane is another desirable requirement for practical application in the field of water treatment [8]. The reusability of the Ag/AgBr/TNF composites for MB degradation were evaluated. Experimental results in Fig. 12 show that the photocatalytic activity has no obvious decrease after five recycles, demonstrating the good stability and reusability of the multifunctional Ag/AgBr/TNF membrane.

Table 1
Summary of the reactions in the photocatalytic process.

Type	Reactions	
electron/hole pair generation	$AgBr + hv \rightarrow AgBr\left(e^- + h^+\right)$	(1)
	$Ag + hv \rightarrow Ag\left(e^- + h^+\right)$	(2)
electron/hole pair separation	$AgBr\left(e^-\right) + Ag \rightarrow AgBr + Ag\left(e^-\right)$	(3)
	$Ag\ e^- + TiO_2 \rightarrow Ag + TiO_2\ e^-$	(4)
active species generation	$TiO_2\left(e^-\right) + O_2 \rightarrow {}^{\bullet}O_2^- + TiO_2$	(5)
	$Ag\left(e^-\right) + O_2 \rightarrow {}^{\bullet}O_2^- + Ag$	(6)
	$AgBr\left(e^-\right) + O_2 \rightarrow {}^{\bullet}O_2^- + AgBr$	(7)
	$AgBr\left(h^+\right) + H_2O \rightarrow AgBr + H^+ + {}^{\circ}OH$	(8)
	$Ag\left(h^+\right) + H_2O \rightarrow Ag + H^+ + {}^{\circ}OH$	(9)
	$Ag/AgBr\left(h^+\right) + r \rightarrow Ag/AgBr + Br^0$	(10)
MB degradation	${}^{\bullet}O_2^-, +MB \rightarrow Degradedproduct$	(11)
	${}^{\circ}OH + MB \rightarrow Degradedproduct$	(12)
	$h^+ + MB \rightarrow Degradedproduct$	(13)
	$Br^0 + MB \rightarrow Degradedproduct + Br^-$	(14)
	$Ag^+ + Br^- \rightarrow AgBr$	(15)

The stability of these photocatalysts could be strongly associated with the charge transfer mechanism in the Ag/AgBr/TNF composites. The AgX is seldom reported to be used as photocatalysts because the photogenerated electron will combine with a mobile interstitial Ag ion leading to separation of Ag atom and the ultimate formation of Ag cluster. In the Ag/AgBr/TNF composite, the presence of metal Ag can effectively inhibit the decomposition of AgBr under simulated visible light irradiation. Because the localized SPR absorption of AgNPs lies in the visible region, the Ag^+ ions inside of the AgBr microspheres will stop being reduced when the surface of AgBr microspheres are covered by a layer of AgNPs.

3.5. Proposed mechanism on the high photocatalytic activity

It is of great importance to reveal the mechanism of high photocatalytic activity behind the Ag/AgBr/TNF composites. The main oxidative species in the photocatalytic process could be detected through the trapping experiments of carriers. The generation and roles of reactive oxidative species (ROS) in the photocatalytic degradation of MB were investigated indirectly with the use of appropriate quenchers of these species. The effects of DMSO (electron scavenger, •OH scavenger) [61], and EDTA (holes scavenger)[47,57] on the photocatalytic degradation rate of MB under visible light irradiation were investigated and the results are shown in Fig. 13. Fig. 13 shows that the MB degradation was greatly suppressed by EDTA, while the degradation rate was slightly less decreased by the added DMSO. These results indicate that the photogenerated holes in the Ag/AgBr/TNF composite might be the main active species in the photocatalytic degradation process of MB.

The possible mechanism for the high stability and visible light photocatalytic activity of the Ag/AgBr/TNF are proposed (Fig. 14). Accordingly, the relevant reactions occurred at the composites surfaces involved in the MB degradation process under visible light irradiation are shown in Table 1. There are holes (h^+), electrons (e^-), ROS like ${}^{\bullet}O_2{}^-$ and hydroxyl radicals (•OH) that are active to oxidize organic pollutants in a photocatalytic process. We presume that there are four kinds of reactions in the present Ag/AgBr/TNF composite under visible light irradiation: (1) electron/hole pair generation; (2) electron/hole pair separation; (3) active species generation; and (4) MB degradation.

Due to the strong SPR in the visible and near-infrared regions AgNPs in the Ag/AgBr/TNF composite can capture photon to generate electron/hole pairs. It is also well known that AgBr can be effectively excited by visible light [56] to generate electron/hole pairs. Hence, both of the SPR of AgNPs and excitation of AgBr could occur in the Ag/AgBr/TNF composite under visible light irradiation. In the present Ag/AgBr/TNF composite, the plasmon-induced electrons on AgNPs might flow to the conduction band (CB) of TiO_2 rather than AgBr, owing to the less negative CB edge of TiO_2 (0.10 V *vs.* NHE) as compared to that of AgBr (1.04 V *vs.* NHE) [58]. Meanwhile, the plasmon-induced holes would migrate away from the AgNPs and be trapped within the surface of AgBr particles, leading to the efficient charge separation in the AgNPs. Besides, the electrons from the photo-excited AgBr could be injected into the AgNPs and immediately transfer to the CB of TiO_2. The electron migration away from AgBr could significantly inhibit the reaction where Ag^+ of AgBr might capture CB electrons to guarantee the stability of the composite. The injection of electrons into the CB of TiO_2, capture of electrons by AgNPs and transfer of holes from AgNPs to valence band (VB) of AgBr not only reduce the electron/hole recombination rate probability, but also greatly improve the stability of AgBr [45]. Therefore, there is a synergetic effect among TiO_2, AgBr and AgNPs in the investigated nanocomposites, which is favorable to the visible light photocatalytic activity of Ag/AgBr/TNF composites [46].

In the active species generation process, the electrons on the surface of TNF, AgBr and AgNPs can reduce the dissolved oxygen on the surface of composites to produce super oxygen anionic free radicals ${}^{\bullet}O_2{}^-$. The holes on AgNPs and AgBr nanoparticles can oxidize H_2O to the hydroxyl radicals ·OH. The radicals of ${}^{\bullet}O_2{}^-$ and •OH can degrade the organic pollutants present at or near the surface of Ag/AgBr/TNF [47]. Furthermore, the holes in the VB of AgBr could reduce the Br^- ions in AgBr to produce Br^0, which is another kind of strong oxidant [46]. The Br^0 can oxidize the MB to the degraded product while changing itself to the Br^- again. The Ag^+ ions in AgBr and the oxidant product Br^- can combine together, in which the stability of AgBr was guaranteed [46].

4. Conclusions

Here, we reported a green approach to develop multifunctional Ag/AgBr/TNF membrane for photocatalytic degradation of pollutants and disinfection of bacteria under visible light irradiation and concurrent water filtration. The Ag/AgBr/TNF composites were synthesized via a low temperature hydrothermal process followed by chemical etching and reaction. The assembled multifunctional Ag/AgBr/TNF membrane showed significantly enhanced disinfection capability towards *E. coli* and photocatalytic degradation activity of pollutant under visible light irradiation compared with pure TNF membrane and commercial P25 NP deposited membrane.

A systematic mechanism explanation investigation showed that the photogenerated holes were found to play a more important role than that of electrons and hydroxyl radicals. There is a synergetic effect among TiO_2, AgBr and AgNPs in the investigated composites. AgBr was the main active component in the Ag/AgBr/TNF composite to generate electron/hole pairs, which were then effectively separated to facilitate the enhancement of photocatalytic process. The AgNPs were another active component that can be excited by visible light to generated electron/hole pairs while simultaneously as an electron-transfer media to ensure the stability of the photocatalyst. The TNF also participated in the charge transfer besides serving as support for Ag/AgBr composites. Besides, both the photocatalytic activity of Ag/AgBr/TNF and its assembled multifunctional membrane exhibited excellent reusability. In view of this, it is reasonable to believe that this study multifunctional Ag/AgBr/TNF membrane is of great significance in promoting the fast development of visible light responsive multifunctional membrane for pollutant degradation, bacteria disinfection and concurrent water filtration for practical engineering applications.

Acknowledgements

Authors would like to acknowledge the financial support (Grant No. NRF2007EWT-CERP01-0420) under Clean Energy Research Programme, National Research Foundation of Singapore. We would also like to thank CESEL and Facts for the use of XRD, FESEM and TEM.

Appendix A. Supplementary data

Supplementary data associated with this article can be found, in the online version, at http://dx.doi.org/10.1016/j.apcatb.2016.05.023.

References

[1] J. Yeston, R. Coontz, J. Smith, C. Ash, Science 313 (2006) 1067.
[2] M.A. Shannon, P.W. Bohn, M. Elimelech, J.G. Georgiadis, B.J. Marinas, A.M. Mayes, Nature 452 (2008) 301–310.
[3] R.P. Schwarzenbach, B.I. Escher, K. Fenner, T.B. Hofstetter, C.A. Johnson, U.V. Gunten, B. Wehrli, Science 313 (2006) 1072–1077.
[4] T. Oki, S. Kanae, Science 313 (2006) 1068–1072.
[5] C.J. Vörösmarty, P. Green, J. Salisbury, R.B. Lammers, Science 289 (2000) 284–288.
[6] P.H. Gleick, PNAS 107 (2010) 21300–21305.
[7] S. Piao, P. Ciais, Y. Huang, Z. Shen, S. Peng, J. Li, L. Zhou, H. Liu, Y. Ma, Y. Ding, P. Friedlingstein, C. Liu, K. Tan, Y. Yu, T. Zhang, J. Fang, Nature 467 (2010) 43–51.
[8] H. Bai, X. Zan, J. Juay, D.D. Sun, J. Membr. Sci. 475 (2015) 245–251.
[9] H. Bai, Z. Liu, L. Liu, D.D. Sun, Chem. Eur. J. 19 (2013) 3061–3070.
[10] H. Bai, L. Liu, Z. Liu, D.D. Sun, Water Res. 47 (2013) 4126–4138.
[11] D. Qin, Z. Liu, D.D. Sun, X. Song, H. Bai, Sci. Rep. 5 (2015) 14530.
[12] S.S. Lee, H. Bai, L. Zhaoyang, D.D. Sun, Environ. Sci. Technol. 49 (2015) 2541–2548.
[13] H. Bai, Z. Liu, D.D. Sun, ChemPlusChem 77 (2012) 941–948.
[14] W.-W. Li, H.-Q. Yu, B.E. Rittmann, Nature 528 (2015) 29–31.
[15] S. Casani, M. Rouhany, S. Knøchel, Water Res. 39 (2005) 1134–1146.
[16] D. Mara, Water Res. 47 (2013) 2105–2117.
[17] B. Volesky, Water Res. 41 (2007) 4017–4029.
[18] H. Steve, Water Res. 43 (2009) 2057–2092.
[19] H. Bai, Z. Liu, D.D. Sun, S.H. Chan, Energy 76 (2014) 607–613.
[20] P. Poizot, F. Dolhem, Energy Environ. Sci. 4 (2011) 2003–2019.
[21] H. Bai, K.S.Y. Kwan, Z. Liu, X. Song, S.S. Lee, D.D. Sun, Appl. Catal. B: Environ. 129 (2013) 294–300.
[22] F. Liu, N.A. Hashim, Y. Liu, M.R.M. Abed, K. Li, J. Membr. Sci. 375 (2011).
[23] H. Bai, Z. Liu, D.D. Sun, Chem. Commun. 46 (2010) 6542–6544.
[24] G.-d. Kang, Y.-m. Cao, J. Membr. Sci. 463 (2014) 145–165.
[25] F. Meng, S.-R. Chae, A. Drews, M. Kraume, H.-S. Shin, F. Yang, Water Res. 43 (2009) 1489–1512.
[26] H. Bai, D.D. Sun, Water Sci. Technol. Water Supply 11 (2011) 324–332.
[27] H. Bai, X. Zan, L. Zhang, D.D. Sun, Sep. Purif. Technol. 156 (Part (3)) (2015) 922–930.
[28] H. Bai, Z. Liu, D.D. Sun, Appl. Catal. B: Environ. 111–112 (2012) 571–577.
[29] R. Wang, K. Hashimoto, A. Fujishima, Nature 388 (1997) 431–432.
[30] F. Liu, M.R.M. Abed, K. Li, J. Membr. Sci. 366 (2011) 97–103.
[31] W. Zhang, Y. Zhu, X. Liu, D. Wang, J. Li, L. Jiang, J. Jin, Angew. Chem. Int. Ed. 53 (2014) 856–860.
[32] A. Fujishima, K. Honda, Nature 238 (1972) 37–38.
[33] T. Paul, P.L. Miller, T.J. Strathmann, Environ. Sci. Technol. 41 (2007) 4720–4727.
[34] R. Asahi, T. Morikawa, T. Ohwaki, K. Aoki, Y. Taga, Science 293 (2001) 269–271.
[35] S. Ramakrishna, R. Jose, P.S. Archana, A.S. Nair, R. Balamurugan, J. Venugopal, W.E. Teo, J. Mater. Sci. 45 (2010) 6283–6312.
[36] L. Huang, J.T. Arena, S.S. Manickam, X. Jiang, B.G. Willis, J.R. McCutcheon, J. Membr. Sci. 460 (2014) 241–249.
[37] L. Liu, Z. Liu, H. Bai, D.D. Sun, Water Res. 46 (2012) 1101–1112.
[38] S. Obregón, Y. Zhang, G. Colón, Appl. Catal. B: Environ. 184 (2016) 96–103.
[39] T. Fotiou, T.M. Triantis, T. Kaloudis, K.E. O'Shea, D.D. Dionysiou, A. Hiskia, Water Res. 90 (2016) 52–61.
[40] S. Liu, Z.R. Tang, Y. Sun, J.C. Colmenares, Y.J. Xu, Chem. Soc. Rev. 44 (2015) 5053–5075.
[41] J.-F. Guo, B. Ma, A. Yin, K. Fan, W.-L. Dai, J. Hazard. Mater. 211–212 (2012) 77–82.
[42] Y. Hu, X. Song, S. Jiang, C. Wei, Chem. Eng. J. 274 (2015) 102–112.
[43] S. George, S. Pokhrel, Z. Ji, B.L. Henderson, T. Xia, L. Li, J.I. Zink, A.E. Nel, L. Mädler, J. Am. Chem. Soc. 133 (2011) 11270–11278.
[44] Y. Wang, L. Liu, L. Xu, C. Meng, W. Zhu, J. Appl. Phys. 113 (2013).
[45] X. Wang, T.T. Lim, Water Res. 47 (2013) 4148–4158.
[46] P. Wang, Y. Tang, Z. Dong, Z. Chen, T.T. Lim, J. Mater. Chem. A 1 (2013) 4718–4727.
[47] Y. Hou, X. Li, Q. Zhao, G. Chen, C.L. Raston, Environ. Sci. Technol. 46 (2012) 4042–4050.
[48] G. Li, X. Nie, J. Chen, Q. Jiang, T. An, P.K. Wong, H. Zhang, H. Zhao, H. Yamashita, Water Res. (2015).
[49] N. Zhang, M.-Q. Yang, S. Liu, Y. Sun, Y.-J. Xu, Chem. Rev. 115 (2015) 10307–10377.
[50] Y. Zhang, Z.R. Tang, X. Fu, Y.J. Xu, Appl. Catal. B: Environ. 106 (2011) 445–452.
[51] X. Zan, H. Bai, C. Wang, F. Zhao, H. Duan, Chem. A Eur. J. 22 (2016) 5204–5210.
[52] H. Bai, Z. Liu, D.D. Sun, J. Am. Ceram. Soc. 96 (2013) 942–949.
[53] H. Bai, J. Juay, Z. Liu, X. Song, S.S. Lee, D.D. Sun, Appl. Catal. B: Environ. 125 (2012) 367–374.
[54] S.S. Lee, H. Bai, Z. Liu, D.D. Sun, Int. J. Hydrogen Energy 37 (2012) 10575–10584.
[55] X. Zhang, A.J. Du, P. Lee, D.D. Sun, J.O. Leckie, J. Membr. Sci. 313 (2008) 44–51.
[56] M.R. Elahifard, S. Rahimnejad, S. Haghighi, M.R. Gholami, J. Am. Chem. Soc. 129 (2007) 9552–9553.
[57] L.S. Zhang, K.H. Wong, H.Y. Yip, C. Hu, J.C. Yu, C.Y. Chan, P.K. Wong, Environ. Sci. Technol. 44 (2010) 1392–1398.
[58] A. Fujishima, X. Zhang, D.A. Tryk, Int. J. Hydrogen Energy 32 (2007) 2664–2672.
[59] Q. Li, S. Mahendra, D.Y. Lyon, L. Brunet, M.V. Liga, D. Li, P.J.J. Alvarez, Water Res. 42 (2008) 4591–4602.
[60] M.N. Chong, B. Jin, C.W.K. Chow, C. Saint, Water Res. 44 (2010) 2997–3027.
[61] I.A. Shkrob, M.C. Sauer, J. Phys. Chem. B 108 (2004) 12497–12511.